Interface between a Liquid Crystalline Polymer and a Flexible Polymer

Xianfeng Li and Morton M. Denn*

The Benjamin Levich Institute for Physico-Chemical Hydrodynamics, City College of the City University of New York, Convent Avenue and 140th Street, New York, New York 10031

Received March 19, 2002; Revised Manuscript Received May 28, 2002

ABSTRACT: The properties of the interfacial region between melt phases of a liquid crystalline polymer and a flexible polymer were studied using the three-dimensional bond fluctuation model. The far-field orientation has a strong effect on the magnitude of the interfacial tension and the structure of the "interphase". The interfacial tension is an increasing function of the nematic order parameter S for a parallel far field, while it is a decreasing function for a homeotropic (orthogonal) far field, with the difference in the magnitude of the interfacial tension growing exponentially in S. The interfacial tension for both far-field orientations is insensitive to liquid crystalline polymer chain length. Chain ends penetrate the adjacent phase with a homeotropic orientation, resulting in a more diffuse interphase. There is, nevertheless, a substantial orientation parallel to the interface even with a homeotropic far field, and order parallel to the interface is induced in the flexible polymer phase with both parallel and homeotropic far fields. The computed parameters for the continuum theory of nematic/isotropic interfaces lead to an "easy axis" that is orthogonal to the interface. The interfacial tension for a parallel far field scales linearly with $(\epsilon/k_BT)^{1/2}S^2$, where ϵ is the magnitude of the repulsive interaction between unlike chain segments; similar scaling is not obtained for an orthogonal far field.

I. Introduction

Polymer blends with a melt-processable liquid crystalline polymer (LCP) dispersed phase are of technological interest, because the LCP inclusions can form a fibrillar morphology during processing, leading to a "self-reinforced" composite with outstanding mechanical properties;[1,2] a dispersed LCP phase can also act as a "flow modifier" during melt extrusion, causing a large decrease in pressure drop.[3] The macroscopic properties of immiscible polymer blends are strongly influenced by the properties of the "interphase", the region of molecular dimension where the two phases meet. Liquid crystalline polymers contain an intrinsic length scale associated with nematic order, namely the correlation length over which the liquid crystalline order is preserved; this scale is of the order of a few micrometers in LCPs and can thus be comparable to the size of the droplets when an LCP is dispersed in a thermoplastic polymer matrix. The nematic order of the LCP can therefore affect the interphase structure, which in turn can affect macroscopic properties and performance of the material; the mechanical response of a blend appears to depend on the size of the LCP droplets relative to the correlation length, for example, possibly because of the effect of nematic order in the small droplets on the interfacial tension, and the droplet dynamics scale differently from those of a flexible polymer in the same matrix.[4]

The interfacial properties of blends of flexible thermoplastic polymers have been studied extensively,[5−9] but the interface in blends containing one or more liquid crystalline polymer phases has received little attention. The Cahn−Hilliard phenomenological theory[10] predicts that the interfacial tension between two amorphous phases is proportional to the square of the concentration gradient. We would also expect a dependence on the scalar order parameter S when one phase is a nematic LCP made up of semiflexible chains, where S is defined as

$$S = \langle 3\cos^2\phi_i - 1\rangle/2 \tag{1}$$

ϕ_i is the angle between the ith bond vector and the LCP director and $\langle\cdots\rangle$ denotes the ensemble average; S varies from 0 for random coils to 1 for perfectly oriented chains. The interface between a flexible polymer and an ordered LCP is expected to be narrow, since the ordered nematic phase strongly excludes the flexible polymer segments, with complete immiscibility in the limit in which the nematic polymer consists of perfectly rigid rods.[11] A continuum model for a nematic−isotropic interface, in which the interfacial free energy density F is a function only of a nematic director $\mathbf{n}$ with unit magnitude, the unit normal to the interface $\mathbf{k}$, and the temperature T, is given by[12,13]

$$F(\mathbf{n}\cdot\mathbf{k},T) = \sigma_i(T) + \sigma_n(\mathbf{n}\cdot\mathbf{k},T) \tag{2}$$

where σ_i is the isotropic interfacial tension and σ_n the anisotropic contribution, known as the *anchoring energy*. σ_n can be expressed in terms of two isotropic functions of temperature:

$$\sigma_n(\mathbf{n}\cdot\mathbf{k},T) = \sigma_2(T)[\mathbf{n}\cdot\mathbf{k}]^2 + \sigma_4(T)[\mathbf{n}\cdot\mathbf{k}]^4 \tag{3}$$

σ_i is of the order of 10 mN/m for low molar mass liquid crystals, while σ_n varies from 10^{-4} to 1 mN/m. Such data are unavailable for nematic LCPs. The director orientation that minimizes F is known as the *easy axis* of the interface. When both σ_2 and σ_4 are positive, the easy axis is along the surface, and the preferred orientation is planar; when both coefficients are negative, the easy axis is orthogonal to the interface and the preferred orientation is homeotropic. The easy axis is at an oblique

10.1021/ma020428d CCC: $22.00
Published on Web 06/29/2002

angle defined by $\mathbf{n}\cdot\mathbf{k} = (-\sigma_2/2\sigma_4)^{1/2}$ when $-1 < \sigma_2/2\sigma_4 < 0$ and $\sigma_2 < 0$.[12]

The isotropic−nematic interfacial tension for rodlike polymer solutions can be calculated using Onsager's[14] energy density expression.[15−17] Doi and co-workers[16] used hyperbolic tangents as trial functions for the interfacial concentration profile and the Onsager trial function for the orientation distribution function, leading to the following expression for the interfacial tension σ:

$$\sigma = 0.257 \frac{k_B T}{d l}[1 + 1.75(\mathbf{n}\cdot\mathbf{k})^2]^{1/2} \quad (4)$$

d and l denote the diameter and length of the rod, respectively. This model predicts that the easy axis is always parallel to the interface ($\mathbf{n}\cdot\mathbf{k} = 0$). Atomistic molecular dynamics calculations for the nematogen 4-pentyl-4′-cyanobiphenyl (5CB) at the surface of amorphous polyethylene, however, indicate nearly homeotropic anchoring.[18] Density functional theory calculations show that the orientational order of semiflexible polymers at a surface can be controlled by changing the nature of a second incompatible liquid.[19,20]

Neutron reflectivity experiments[5,21] show that the interfacial profile is broadened by capillary waves, which are long wavelength thermal oscillations developing about the equilibrium interfacial plane with probability $\exp(-\beta A)$,[22] where A is the Helmholtz free energy. The free energy can be resolved into two components: the "intrinsic" mean-field energy of the unperturbed interface and the reversible work associated with the creation of undulations. This separation assumes that the undulations are of sufficiently small wavelength so as not to modify the intrinsic structure. Hence, there are two characteristic interfacial length scales: the intrinsic width, over which the density of a planar interface changes from one bulk value to the other, and the capillary wave dispersion of the planar interface arising from fluctuations. The total interfacial width for isotropic phases, according to the results of Lacasse and co-workers,[9] is

$$w^2 = {w_0}^2 + \frac{k_B T}{2\pi\sigma} \ln\left(\frac{L}{c w_0}\right) \quad (5)$$

where w_0 is related to the intrinsic interfacial width, L is the linear size of the system, and c is a constant. The leading order terms for the capillary fluctuation Hamiltonian,[23] which reflects the free energy cost of deviations from a planar interface in the $x-y$ plane, are written

$$H = \int \left\{ \frac{\sigma}{2}[\nabla h(\mathbf{x})]^2 + \frac{\kappa}{2}[\nabla^2 h(\mathbf{x})]^2 + ... \right\} \mathrm{d}x\, \mathrm{d}y \quad (6)$$

κ is the interfacial bending modulus. The local interfacial position $h(\mathbf{x})$ is traced by a ghost particle[24] in the interfacial region at each (x,y), where it feels repulsive interactions from A- and B-monomers within a range of $\sqrt{6}$ in lattice space. The interface corresponds to the position where the ghost particle experiences the minimum thermal interactions. $h(\mathbf{x})$ is then decomposed as

$$h(\mathbf{x}) = \frac{a_0}{2} + \sum_{l_x=-L_x/2}^{L_x/2} \sum_{l_y=-L_y/2}^{L_y/2} a(\mathbf{q}) \exp(i\mathbf{q}\cdot\mathbf{x}) \quad (7)$$

with complex Fourier components $a(\mathbf{q})$ and wave vectors $q_x = 2\pi l_x/L_x$, $q_y = 2\pi l_y/L_y$. It then follows from the equipartition theorem that

$$\frac{2k_B T}{L_x L_y \langle a(q)^2 \rangle} = \sigma q^2 + \kappa q^4 + ... \quad (8)$$

where $\langle a(q)^2 \rangle$ is the mean-square value of the Fourier coefficients. The interfacial tension thus follows from the slope of $\langle a(q)^2 \rangle^{-1}$ as a function of q^2 for small q^2.

In this paper, we employ three-dimensional Monte Carlo simulations to study the equilibrium "interphase" structure and interfacial tension of a flexible/semiflexible polymer melt blend, using the bond fluctuation model[25] and the capillary wave theory. The bond fluctuation model and the simulation technique are described in section II. A detailed investigation of the interfacial properties for a symmetric blend is presented in section III, where the equilibrium properties are investigated for various liquid crystalline orders and interactions between heterogeneous phases. The connection between the Monte Carlo calculations and the continuum theory is addressed in section IV, while the effects of chain length and polydispersity of the LCP phase are discussed in section V. Section VI contains the conclusions.

II. Simulation Model

We focus on the effects of chain orientation, bulk nematic order, and interaction between unlike species on the structure of the interface between a liquid crystalline polymer (polymer A) and a flexible polymer (polymer B), using the three-dimensional bond fluctuation model (BFM)[25] in Monte Carlo calculations. The BFM has been used to study the interfacial region between blends of flexible polymers,[6−8] the dynamics of a LCP,[26,27] and the interfacial region between polymers of different degrees of stiffness.[28,29] Some preliminary results applying the BFM to the interface between a LCP and a flexible polymer were reported in ref 30. In the framework of the model, each monomer occupies eight sites of a unit cell in a simple cubic lattice. Monomers along a chain are connected via one of 108 bond vectors, within the set

$$\mathbf{B} = P(2,0,0) \cup P(2,1,0) \cup P(2,1,1) \cup P(2,2,1) \cup P(3,0,0) \cup P(3,1,0) \quad (9)$$

where $P(a,b,c)$ stands for the set of all permutations and sign combinations of $\pm a$, $\pm b$, $\pm c$. The allowable bond length can therefore take any one of the five values 2, $\sqrt{5}$, $\sqrt{6}$, 3, and $\sqrt{10}$ (in units of lattice spacing). A randomly selected monomer can jump to one of six nearest lattice neighbors; a permissible jump must satisfy the excluded-volume constraint to avoid overlap of monomers at the same lattice site and the bond length constraint to avoid intersections of chain segments.

The amorphous polymers and the LCPs were characterized in the simulations as random coils and semirigid chains, respectively, with a pairwise repulsive interaction between unlike monomers that are within $\sqrt{6}$ lattice units. The far-field orientation of the LCP was set by imposing an orientational field. Two far-field orientations were considered for most simulations, motivated by the equilibrium states in a spherical droplet of a rigid nematic:[31] a homeotropic orientation, in which the LCP is normal to the mean interface (corresponding to a "hedgehog" structure in a droplet,

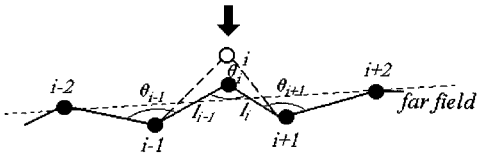

Figure 1. Schematic description of the move involved in the Monte Carlo process.

with a point disclination at the center), and an orientation parallel to the mean interface (corresponding to a dipolar, or "boojum", structure in a droplet, with point disclinations at the poles). Only the excluded-volume effect was considered for the amorphous phase, whereas two energetic interactions were considered for the LCP phase: (i) the intrachain bending energy, equal to $E_{b0}(1 + \cos \theta_i)^2$, where θ_i is the angle between successive bonds, and (ii) the orientational energy between LCP segments and the orientational field, equal to $E_{f0} \sin^2 \phi_i$, where ϕ_i is the angle between the segment and the field directions. Figure 1 shows a typical Monte Carlo move of a LCP monomer; the move simultaneously changes three bond angles, two bond lengths, and the angles between the LCP segments and the orientational field. The Metropolis important sampling criterion[32] was used, wherein the acceptable transition probability $\exp(-\delta E/k_B T)$, where δE is the change of energy, must exceed a random number uniformly distributed between 0 and 1.

The lattice dimensions were $L_x \times L_y \times L_z = 64 \times 64 \times 384$, with periodic boundaries in the $x-y$ plane and hard walls in the z-direction. Sixty-five percent of the lattice sites were occupied; previous simulations based on the BFM have shown that this volume fraction is large enough to represent a polymer melt.[33] The sample volume contained 4000 chains for a symmetric blend with chain lengths $N_A = N_B = 32$. The amorphous and LCP phases occupied $^1/_6$ and $^5/_6$ of the sample volume, respectively. Assuming that a bond in the BFM corresponds to roughly 3−5 chemical monomers in a real polymer,[34] a chain length of 32 corresponds to 96 to 160 real monomers; these chains are clearly too short to describe entanglement dynamics in flow, but they should reflect equilibrium interfacial behavior adequately.[9] When the effects of chain length and polydispersity were considered, the volume fractions occupied by the two phases were not changed and the chain length of the flexible polymer remained unchanged at $N_B = 32$, but LCP chain lengths with $N_A = 8$ and 16 were used, as well as an approximation to the Flory distribution[35] characteristic of polyester LCPs with chain lengths ranging from 8 to 32.

Nematic order in the far field was varied by changing the temperature. E_{b0} and E_{f0} were taken to be equal, with $E_{b0}/k_B T = E_{f0}/k_B T = 1.25$, 1.75, 2.5, 3.75, and 5. Five values of bulk nematic order were thus obtained: $S = 0.36$, 0.59, 0.78, 0.86, and 0.91. The dimensionless repulsive square-well potential $\epsilon/k_B T$, which controls miscibility, was taken equal to 0.625, 1.25, 2.5, 3.75, and 5 at each temperature. The simulation was started from an initial configuration in which the chains in both phases were random coils, corresponding to a system at infinite temperature, followed by a stepwise "slow cooling"[26] that enabled the extension of the LCP chains with decreasing temperature and the development of an organized nematic phase. A total of 5×10^9 Monte Carlo steps were required to reach equilibrium because of the extremely slow dynamics of the interfacial fluctuations; samples were taken thereafter at every 10^6-th successful configuration in the run, and 5000 equilibrium configurations were used in the statistics. Typical equilibrium chain conformations near the interface are shown in parts a and b of Figure 2 for parallel and homeotropic far-field orientations, respectively, with $S = 0.78$ and $\epsilon/k_B T = 2.5$. Chain-end penetration across the interface can be seen in the simulation with a homeotropic far field, whereas chain-end penetration is not an obvious feature of the simulation with a parallel far field.

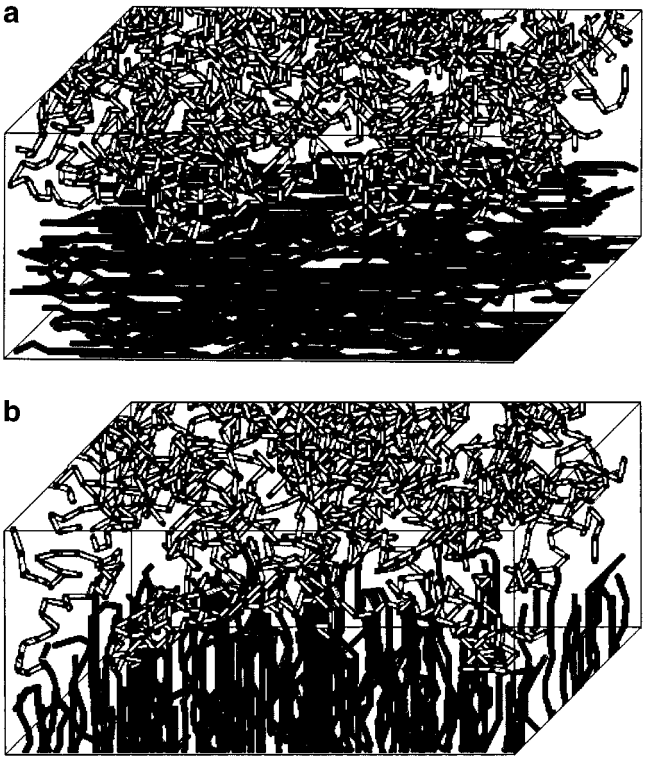

Figure 2. Typical equilibrium configurations under (a, top) parallel and (b, bottom) homeotropic orientation fields, with $S = 0.78$ and $\epsilon/k_B T = 2.5$. The dark chains are the LCPs.

III. Equilibrium Interfacial Properties of Symmetric Blends

A. Chain Orientation near the Interface. The asymmetry parameter, which indicates average orientation relative to a reference direction, is a useful measure of molecular conformation; the reference direction for the LCP is taken as the direction of the molecular field, in which case $\lambda_{n,p}$ and $\lambda_{n,h}$, the asymmetry parameters of the LCP under parallel and homeotropic orientation fields, respectively, are defined as follows:[36]

$$\lambda_{n,p} = \frac{2\langle R_{gx}^2\rangle_z - \langle R_{gy}^2\rangle_z - \langle R_{gz}^2\rangle_z}{2(\langle R_{gx}^2\rangle_z + \langle R_{gy}^2\rangle_z + \langle R_{gz}^2\rangle_z)} \quad (10a)$$

$$\lambda_{n,h} = \frac{2\langle R_{gz}^2\rangle_z - \langle R_{gx}^2\rangle_z - \langle R_{gy}^2\rangle_z}{2(\langle R_{gx}^2\rangle_z + \langle R_{gy}^2\rangle_z + \langle R_{gz}^2\rangle_z)} \quad (10b)$$

$\langle R_{gs}^2\rangle_z$ ($s = x, y, z$) denotes the s component of the mean-square radius of gyration of a chain at position z. The reference direction for the flexible polymer is taken to be the same as that for the LCP for each case, so the asymmetry parameter λ_f is defined by eq 10a when the LCP far-field orientation is parallel to the interface and

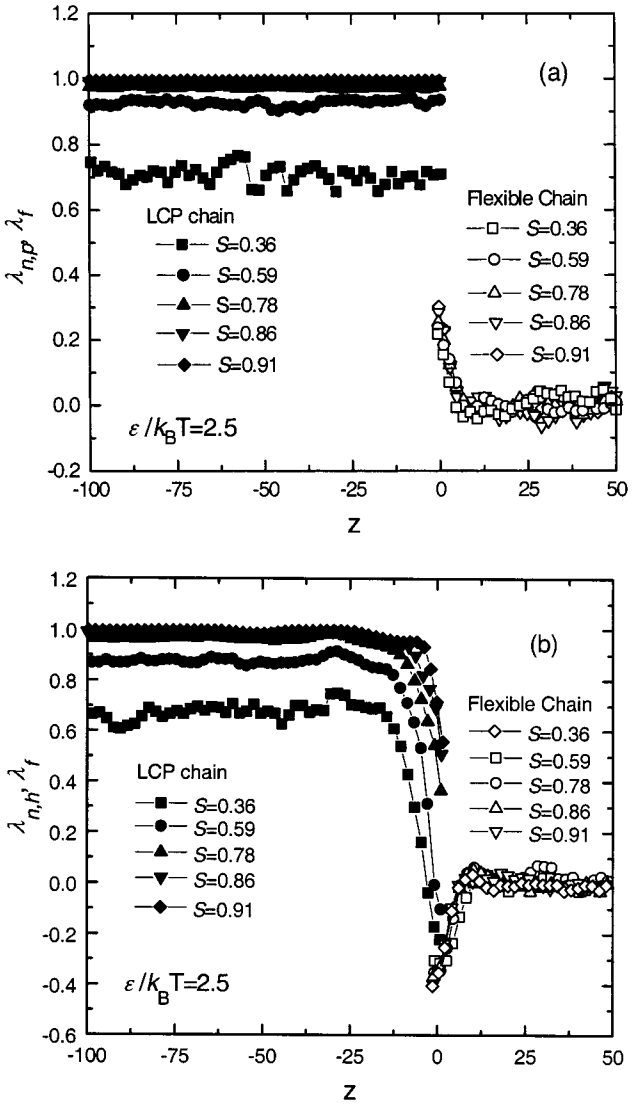

Figure 3. Orientational asymmetry parameters for different LCP order parameters for (a) parallel and (b) homeotropic orientations; $\epsilon/k_BT = 2.5$.

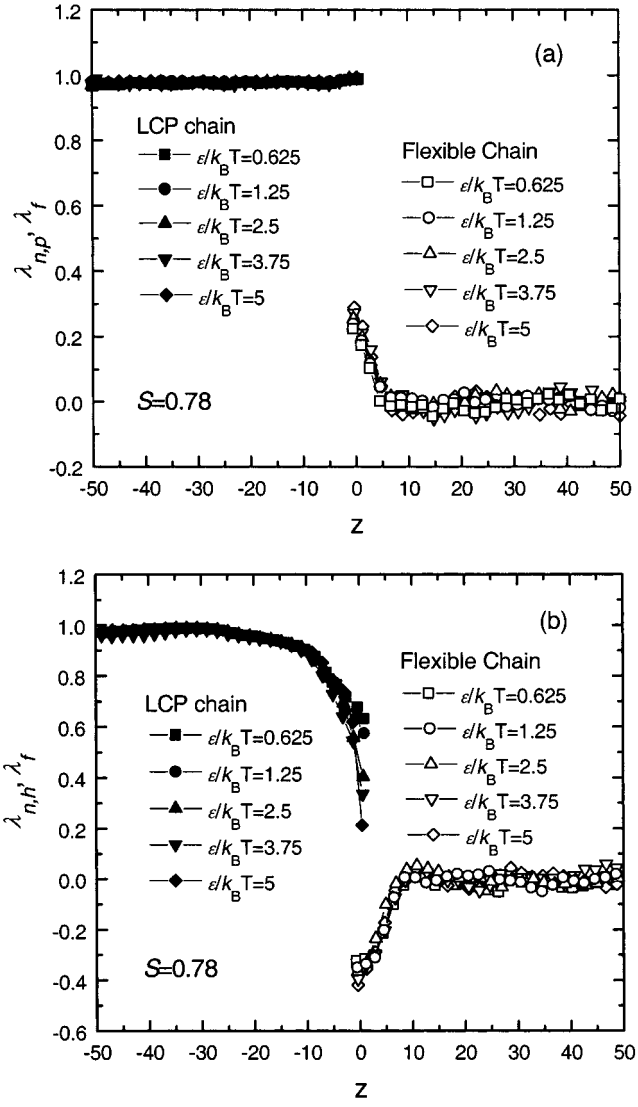

Figure 4. Orientational asymmetry parameters for different repulsive potentials between unlike chain segments for (a) parallel and (b) homeotropic orientations; $S = 0.78$.

by eq 10b when the LCP orientation is homeotropic. The dependence of the asymmetry parameters on the nematic order S with $\epsilon/k_BT = 2.5$ is shown in Figure 3a for the parallel far field and in Figure 3b for the homeotropic far field. The dependence of the asymmetry parameters on ϵ/k_BT for $S = 0.78$ is shown in parts a and b of Figure 4 for parallel and homeotropic far fields, respectively. The asymmetry parameters near the impenetrable walls are not included in these figures; there is induced parallel orientation in the vicinity of the walls,[30] but these regions are always separated from the interface by a region of bulk behavior in each phase. The bulk values of $\lambda_{n,p}$ and $\lambda_{n,h}$ are functions of S for LCP chains, and the values increase to unity with increasing S. In the interfacial region, however, the properties of $\lambda_{n,p}$ and $\lambda_{n,h}$ are dramatically different. The sharp decrease in $\lambda_{n,h}$ for the homeotropic orientation in Figures 3b and 4b indicates that LCP chains that are oriented orthogonal to the interface in the far field deviate from the direction of the orientational field in the interfacial region and move into the plane of the interface; a value of -0.5 would indicate perfect orientation orthogonal to the field. There is no evident out-of-plane movement in Figures 3a and 4a for the chains with a far-field orientation that is parallel to the interface.

λ_f vanishes in the bulk for the amorphous polymer, reflecting the isotropy of the flexible chains, but becomes nonzero within about 1.5 radii of gyration ($R_g = 6.7$ in lattice units) of the mean interface for both far-field LCP orientations, indicating that the LCP phase induces the flexible chain segments to orient parallel to the interface. Isotropy in the plane of the interface would lead to a value of $\lambda_f = 0.25$ in Figures 3a and 4a; the slightly higher value indicates a small bias toward the x-direction.

B. "Interphase" Composition Profile. The mass fraction profiles in the interfacial region were well represented by a hyperbolic tangent,

$$\rho_{LCP}(z) = \frac{1}{2}\left(1 + \tanh\frac{z}{w}\right) \qquad (11)$$

where $\rho_{LCP}(z)$ is the mass fraction of LCP monomers and z is the coordinate orthogonal to the interface. The profiles are shown in Figure 5a for $S = 0.78$ and various values of ϵ/k_BT and in Figure 5b for $\epsilon/k_BT = 2.5$ and various values of S. The interfacial region for the homeotropic far-field orientation is far more diffuse than

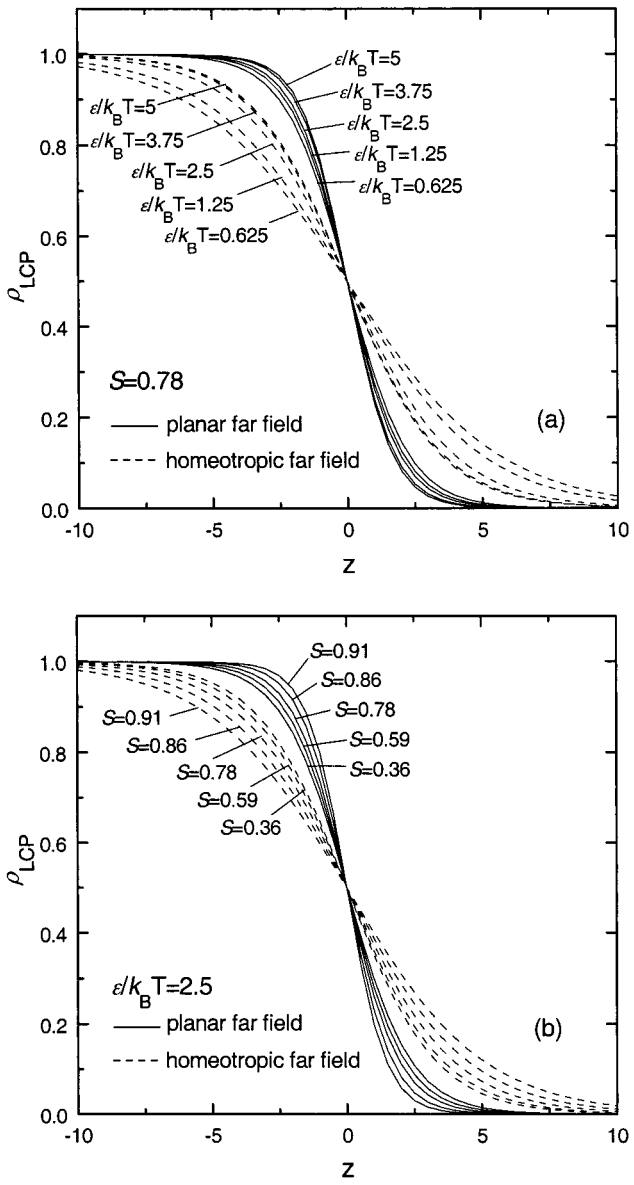

Figure 5. Mass fraction profiles of the LCP for parallel (solid lines) and homeotropic (dashed lines) orientations (a) with $S = 0.78$ for various ϵ/k_BT and (b) with $\epsilon/k_BT = 2.5$ of various values of S.

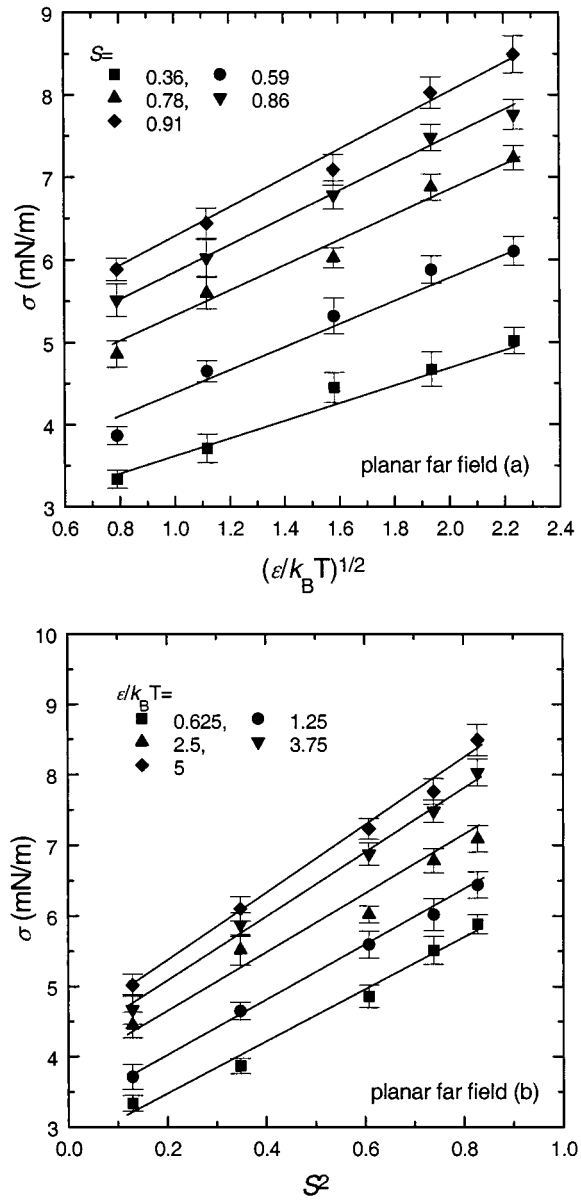

Figure 6. Dependence of the interfacial tension for planar orientations (a) on $(\epsilon/k_BT)^{1/2}$ for various values of S and (b) on S^2 for various values of ϵ/k_BT.

for the parallel orientation, and the profile for the parallel orientation is much less sensitive to the repulsive potential. The interface sharpens with increasing order parameter for the parallel orientation, while it becomes more diffuse with increasing order parameter for the homeotropic orientation. Most of these observations follow readily from the fact that the orthogonal orientation facilitates the penetration of chain ends into both phases, while chain-end penetration becomes increasingly difficult with a parallel orientation as the chains become more rigid. (A perfectly rigid parallel chain of infinite length would prevent any chain-end penetration, so the interfacial width for infinite parallel chains in the limit $S \rightarrow 1$ must be one lattice unit.)

C. Interfacial Tension. The interfacial tension for the parallel far field obtained using the capillary wave theory is shown in Figure 6a as a function of $(\epsilon/k_BT)^{1/2}$ for fixed S and in Figure 6b as a function of S^2 for fixed ϵ/k_BT. The calculated interfacial tensions were converted from lattice units to physical units of mN/m using $k_BT = 4.14 \times 10^{-14}$ erg (room temperature) and a physical lattice spacing of 2 Å.[34] Nonzero values of the bending moment κ were not obtained within the uncertainty of the calculations. The linear dependence of σ in Figure 6a can be rationalized on the basis of the self-consistent-field theory for a binary incompressible blend of infinite Gaussian chains in the strong segregation limit,[37] which predicts that the interfacial tension is proportional to the square root of the Flory−Huggins interaction parameter χ; in the mean-field approximation, χ is proportional to the inverse of the dimensionless temperature k_BT/ϵ. The linearity in S^2 is more difficult to rationalize. The lowest-order representation of the nematic potential scales with S^2, so the free energy difference between the bulk phases can also be expected to scale with S^2; the interfacial width depends on S, however, so there is no apparent reason to expect the free energy gradient to scale with S^2. The calculated free energies are plotted as a function of the product $(\epsilon/k_BT)^{1/2}S^2$ in Figure 7, where it can be seen that there is an excellent linear correlation for $(\epsilon/k_BT)^{1/2}S^2 > 0.4$. The interfacial widths computed from the fits in Figure

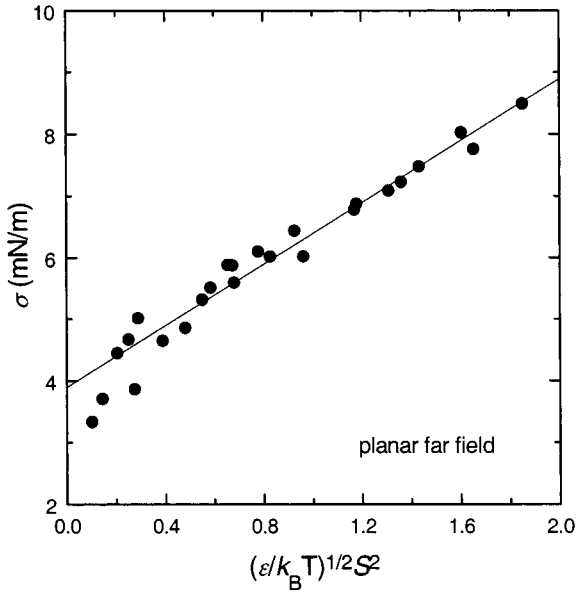

Figure 7. Dependence of interfacial tension on $(\epsilon/k_BT)^{1/2}S^2$ for planar orientations.

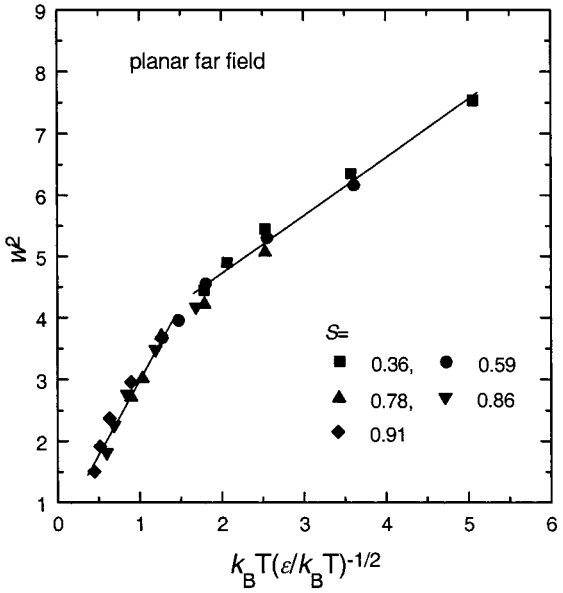

Figure 8. Temperature dependence of the square of interfacial width for planar orientation.

5 are plotted in Figure 8 as w^2 vs $k_BT(\epsilon/k_BT)^{-1/2}$. Superposition of the values of w^2 onto a single curve is partly consistent with the mean-field scaling, but only with the added restriction that the interfacial width in eq 5 is dominated by the capillary wave contribution.

The dependence of the interfacial tension on $(\epsilon/k_BT)^{1/2}$ and S^2 is plotted in parts a and b of Figure 9, respectively, for the homeotropic orientation. There appear to be two regimes in the dependence of σ on the interaction parameter, with a transition in the neighborhood of $\epsilon/k_BT \sim 2$. Unlike the parallel orientation, the interfacial tension is a *decreasing* function of the nematic order parameter, with a transition to a sharper decrease at $S \sim 0.8$. The decrease with increasing S is consistent with the fact that the interface becomes more diffuse with increasing nematic order when the far field is homeotropic. The values of σ do not collapse onto a single curve when plotted as a function of $(\epsilon/k_BT)^{1/2}S^2$. The values do come together somewhat when σ is plotted as a

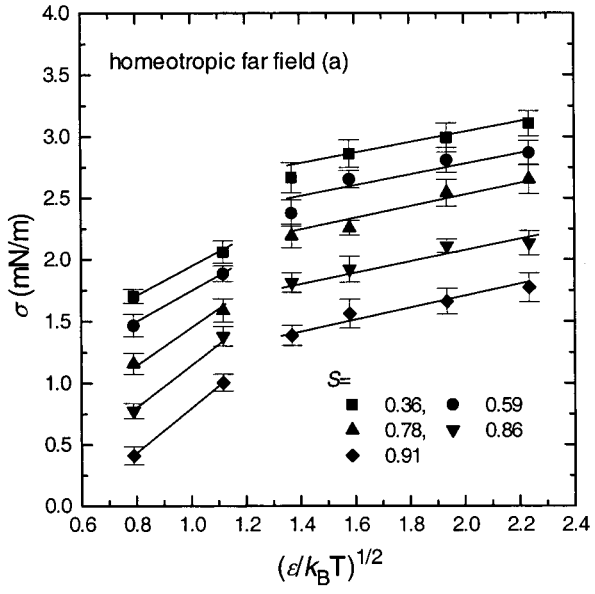

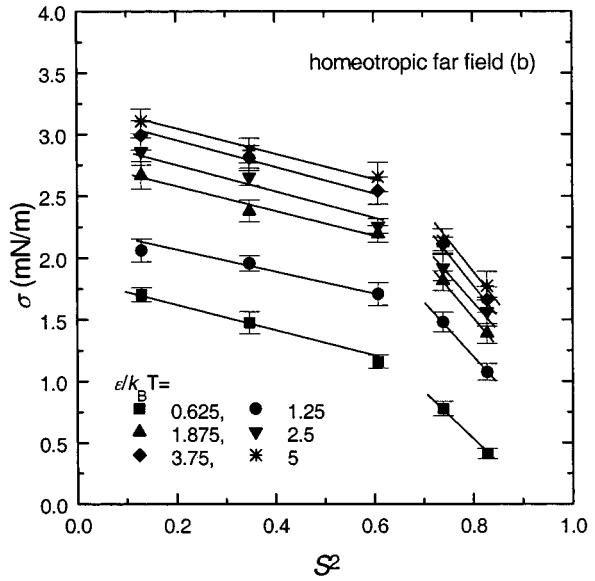

Figure 9. Dependence of the interfacial tension for homeotropic orientations (a) on $(\epsilon/k_BT)^{1/2}$ for various values of S and (b) on S^2 for various values of ϵ/k_BT.

function of $(\epsilon/k_BT)^{1/2}(1 - S^2)$, as shown in Figure 10, but the reason for this scaling is not obvious, and there appear to be two regimes; a single curve is achieved only for large repulsive potentials and small order parameters. The values of w^2 do not collapse when plotted as a function of $k_BT(\epsilon/k_BT)^{-1/2}$, as can be seen in Figure 11.

The difference of σ between the parallel and homeotropic interfacial tensions is relatively insensitive to the repulsive potential and increases rapidly with increasing nematic order, as shown in Figure 12. The results roughly correlate as

$$\Delta\sigma \sim \exp(2.2S) \tag{12}$$

There is no region of power-law behavior, and the difference does not appear to diverge in the limit $S \rightarrow 1$.

IV. Continuum Theory

The continuum theory for the interfacial tension of an isotropic/nematic interface in eqs 4 and 5 contains

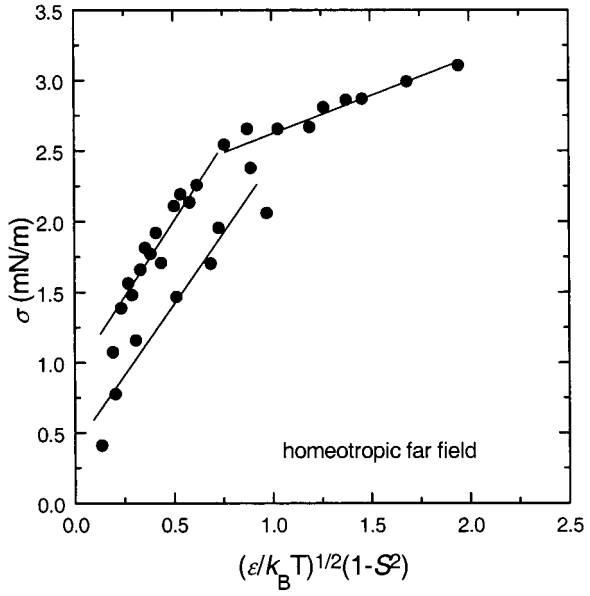

Figure 10. Dependence of the interfacial tension on $(\epsilon/k_BT)^{1/2}(1 - S^2)$ for homeotropic orientations.

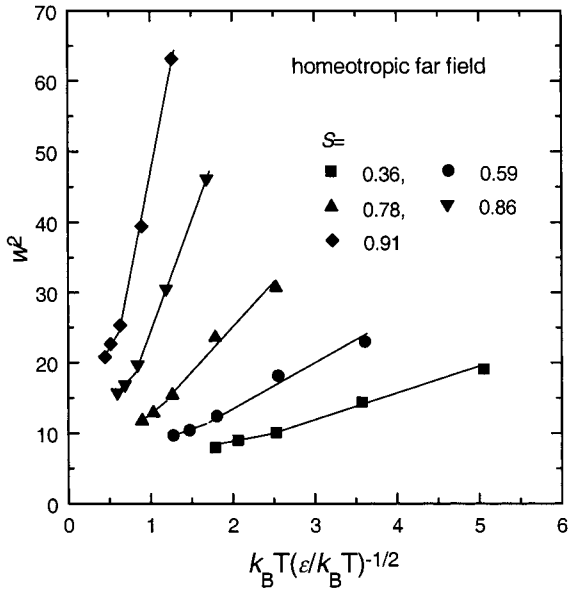

Figure 11. Temperature dependence of the square of interfacial width for homeotropic orientation.

three scalar functions of temperature: σ_i, σ_2, and σ_4. We have carried out additional calculations with a far-field orientational field at an angle $\pi/4$ to the interface and $\epsilon/k_BT = 2.5$ in order to evaluate the three parameters. Values of σ_2 and σ_4 are plotted vs S^2 in Figure 13, where a linear dependence is seen. To a good approximation, $\sigma_2 \sim -2\sigma_4$ for all values of S^2, in which case the "easy angle" is close to zero ($\mathbf{n}\cdot\mathbf{k} \cong 1$) and σ_i is very close to the computed interfacial tension for the parallel orientation; i.e., the homeotropic orientation is preferred in the absence of an imposed far-field orientation. The computed minimizing angles are shown as an inset in Figure 13.

V. Effects of Chain Length and Polydispersity

The effect of LCP chain length on the calculated interfacial tension is shown in Figure 14 for $S = 0.78$, $\epsilon/k_BT = 2.5$, and $N_A = 8$, 16, and 32. The chain length of the flexible polymer was fixed at $N_B = 32$. The

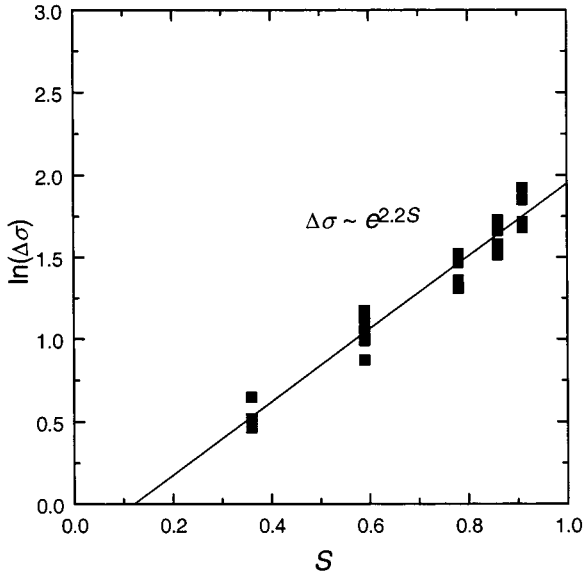

Figure 12. Dependence of the difference of the interfacial tension between planar and homeotropic orientations as a function of S.

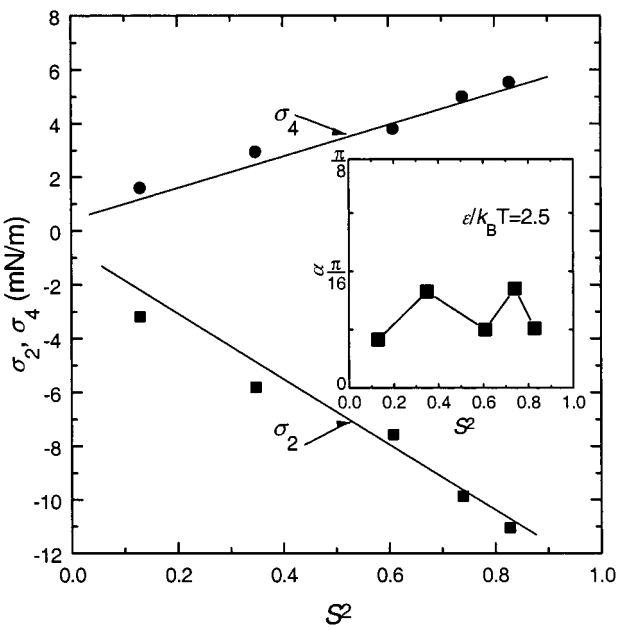

Figure 13. Dependence of σ_2 and σ_4 on S^2 at $\epsilon/k_BT = 2.5$. The computed minimizing angles are shown as an inset.

interfacial tension is very insensitive to chain length for both far-field orientations.

Calculations to determine any effect of LCP polydispersity were carried out for $S = 0.78$ and $\epsilon/k_BT = 2.5$ using the truncated Flory distribution[35] shown in the inset in Figure 15. The number-average chain length for this distribution is 14.2, while the weight-average chain length is 28.2, giving a polydispersity of 1.98. The computed interfacial tension for the two far-field orientations is shown as squares in Figure 14 and reflects the insensitivity of the interfacial tension to LCP chain length. The number-average chain-length distribution in the LCP phase is shown as a function of distance from the interface in Figure 15. The distribution is relatively insensitive to position for the parallel orientation, but there is a marked segregation of shorter chains at both the interface and the hard wall for the homeotropic orientation, with an adjacent enrichment of longer

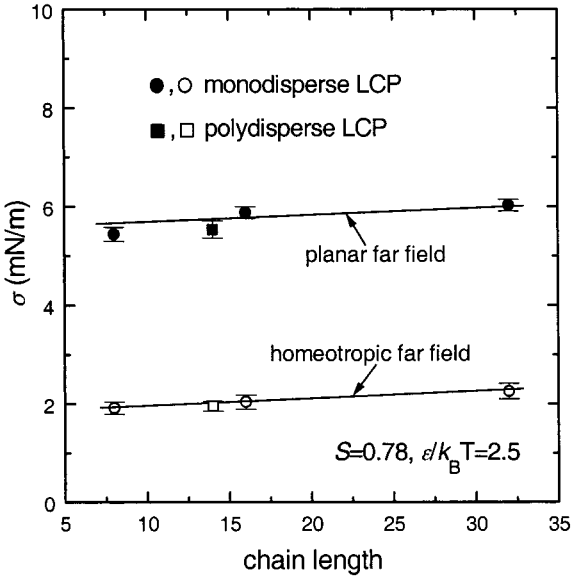

Figure 14. Dependence of interfacial tension on the number-average chain length for $\epsilon/k_BT = 2.5$ and $S = 0.78$. The squares are for the polydisperse LCP.

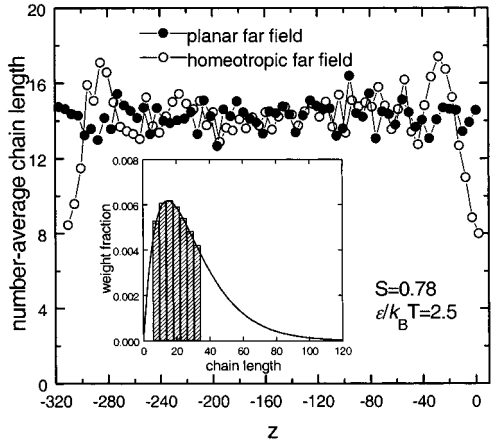

Figure 15. Profiles of number-average LCP chain length as a function of distance from the interface. The solid and open symbols indicate the profiles for planar and homeotropic orientational fields, respectively. The inset shows the chain length distribution for the polydisperse LCP, with a number-average chain length of 14.23 and a polydispersity of 1.98.

chains. Surface segregation of the lower molecular weight component is generally expected,[38] but it is observed here only for the homeotropic far-field orientation.

VI. Conclusions

The far-field orientation has a strong effect on the structure of the "interphase" and the interfacial tension between melt phases of a liquid crystalline polymer and a flexible polymer. The interfacial tension is an increasing function of the nematic order parameter for a parallel far field, while it is a decreasing function of the order parameter for an orthogonal far field, with the difference between the values growing as $\exp(2.2S)$. The "easy axis" is orthogonal to the interface, which agrees with the molecular dynamics simulations[18] of the orientation of a low molar mass liquid crystal at the surface of an amorphous polymer but contradicts a theoretical calculation[16] that predicts a parallel easy axis. The critical factor here seems to be the ability of chain ends with a homeotropic orientation to penetrate the adjacent phase, resulting in a more diffuse interphase. A homeotropic orientation is thus expected in the absence of other orienting fields. There is, nevertheless, substantial equilibrium orientation parallel to the interface even with a homeotropic far field, and substantial order parallel to the interface is induced in the flexible polymer phase over a distance of the order of the radius of gyration with both parallel and homeotropic far fields.

The interfacial tension for a parallel far field scales linearly with $(\epsilon/k_BT)^{1/2}S^2$, and the squared thickness of the interfacial region correlates, albeit nonlinearly, with $k_BT(\epsilon/k_BT)^{-1/2}$. These results are consistent in part with mean-field results for Gaussian chains, which have no nematic order ($S = 0$). Scaling based on the mean-field results is less successful for the homeotropic far field. It is not obvious why the scaling derived from mean-field theory for Gaussian chains should work at all, nor why it is more successful for the parallel orientation than for the orthogonal orientation, since only the latter permits the chain-end penetration that would be expected with Gaussian chains.

Finally, we return to the dynamical experiments on blends with an LCP dispersed phase that motivated this study. One might expect the LCP to adopt the easy angle at the interface and to propagate the homeotropic orientation into the interior, leading in all cases to a "hedgehog" orientation in spherical droplets. The micron-scale correlation length observed in bulk samples of LCP melts is undoubtedly caused by defects that are trapped by entanglements of the semiflexible LCP chains. Hence, internal orienting fields resulting from the defects compete with the preferred orientation at the interface. This effect is likely to be more prevalent in droplets that are large relative to the correlation length, since these droplets will have a large number of defects. Given the exponential dependence of the difference in interfacial tension on nematic order parameter, it is therefore reasonable to assume that the interfacial tension in a large droplet or bulk sample will be substantially larger than the interfacial tension in a small droplet in which the preferred surface orientation is possible. This reasoning is consistent with the empiricism observed in ref 4, in which taking the interfacial tension to be zero for droplets smaller than the correlation length was required to apply the Palierne theory[39] for viscoelastic blends. The reasoning does not take into account interfacial flows that would be induced by gradients in the interfacial tension.

Acknowledgment. This work was supported in part by the donors of the Petroleum Research Fund under Grant ACS-PRF 36563-AC7 and in part by the National Science Foundation under Grant CTS-0112358.

References and Notes

(1) Handlos, A. A.; Baird, D. G. *J. Macromol. Sci., Rev. Macromol. Chem. Phys.* **1995**, *C35*, 183.
(2) Cogswell, F. N.; Griffin, B. P.; Rose, J. B. U.S. Patent No. 4386174, 1983; 4433083, 1984; 4438236, 1984.
(3) Weiss, R. A.; Huh, W.; Nicolais, L. *Polym. Eng. Sci.* **1987**, *27*, 684. Dutta, D.; Fruitwala, H.; Kohli, A.; Weiss, R. A. *Polym. Eng. Sci.* **1990**, *30*, 1005.
(4) Riise, B. L.; Mikler, N.; Denn, M. M. *J. Non-Newtonian Fluid Mech.* **1999**, *86*, 3. Lee, H. S.; Denn, M. M. *J. Rheol.* **1999**, *43*, 1583. Lee, H. S.; Denn, M. M. *J. Non-Newtonian Fluid Mech.* **2000**, *93*, 315.
(5) Sferrazza, M.; Xiao, C.; Jones, R. A. L. *Phys. Rev. Lett.* **1997**, *78*, 3693.

(6) Werner, A.; Schmid, F.; Müller, M.; Binder, K. *J. Chem. Phys.* **1997**, *107*, 8175; *J. Chem. Phys.* **1999**, *110*, 1221; *Phys. Rev. E* **1999**, *59*, 728.
(7) Müller, M.; Schick, M. *J. Chem. Phys.* **1996**, *105*, 8885. Werner, A.; Schmid, F.; Müller, M. *J. Chem. Phys.* **1999**, *110*, 5370.
(8) Müller, M.; Schick, M. *J. Chem. Phys.* **1996**, *105*, 8282.
(9) Lacasse, M. D.; Grest, G. S.; Levine, A. J. *Phys. Rev. Lett.* **1998**, *80*, 309.
(10) Cahn, J. W.; Hilliard, J. E. *J. Chem. Phys.* **1958**, *28*, 258.
(11) Flory, P. J. *Macromolecules* **1978**, *11*, 1138.
(12) Faetti, S. In *Physics of Liquid Crystalline Materials*; Khoo, I.-C., Simoni, F., Eds.; Gordon and Breach: Philadelphia, PA, 1991; Chapter XII, p 301.
(13) Rey, A. D. *Phys. Rev. E* **2000**, *61*, 1540.
(14) Onsager, L. *N.Y. Ann. Acad. Sci.* **1949**, *51*, 627.
(15) Chen, Z. Y.; Noolandi, J. *Phys. Rev. A* **1992**, *45*, 2389.
(16) Doi, M.; Kuzuu, N.; Sato, T.; Teramoto, A. *Macromolecules* **1984**, *17*, 65.
(17) McMullen, W. E. *Phys. Rev. A* **1988**, *38*, 6384.
(18) Doerr, T. P.; Taylor, P. L. *Mol. Cryst. Liq. Cryst.* **1999**, *330*, 1735.
(19) ten Bosch, A. *J. Chem. Phys.* **1998**, *108*, 2228.
(20) ten Bosch, A. *Phys. Rev. E* **2001**, *63*, 061808-1.
(21) Hermes, H. E.; Higgins, J. S.; Bucknall, D. G. *Polymer* **1997**, *38*, 985. Bucknall, D. G.; Butler, S. A.; Hermes, H. E.; Higgins, J. S. *Physica B* **1998**, *241*, 1071.
(22) Croxton, C. A. *Statistical Mechanics of the Liquid Surface*; John Wiley & Sons: New York, 1980.
(23) Helfrich, W. *Z. Naturforsch.* **1973**, *28C*, 693. Canham, P. B. *J. Theor. Biol.* **1970**, *26*, 61. Evans, E. *Biophys. J.* **1974**, *14*, 923.
(24) Laradji, M.; Mouritsen, O. G. *J. Chem. Phys.* **2000**, *112*, 8621.
(25) Carmesin, I.; Kremer, K. *Macromolecules* **1988**, *21*, 2819. Deutsch, H. P.; Binder, K. *J. Chem. Phys.* **1991**, *94*, 2294.
(26) Rodríguez, A. L.; Wittmann, H. P.; Binder, K. *Macromolecules* **1990**, *23*, 4327.
(27) Zhang, H. D.; Yang, Y. L. *Macromolecules* **1998**, *31*, 7550.
(28) Müller, M.; Werner, A. *J. Chem. Phys.* **1997**, *107*, 10764.
(29) Schmid, F.; Müller, M. *Macromolecules* **1995**, *28*, 8639.
(30) Li, X. F.; Denn, M. M. *Phys. Rev. Lett.* **2001**, *86*, 656.
(31) Drzaic, P. S. *Liquid Crystal Dispersions*; World Scientific: Singapore, 1995.
(32) Metropolis, N.; Rosenbluth, A. W.; Rosenbluth, M. N.; Teller, A. N.; Teller, E. *J. Chem. Phys.* **1953**, *21*, 1087.
(33) Paul, W.; Binder, K.; Heermann, D. W.; Kremer, K. *J. Phys. II* **1991**, *1*, 37.
(34) Baschnagel, J.; Binder, K.; Paul, W.; Laso, M.; Suter, U.; Batoulis, I.; Jilge, W.; Bürger, T. *J. Chem. Phys.* **1991**, *95*, 6014.
(35) Flory, P. J. *Principles of Polymer Chemistry*; Cornell University: Ithaca, NY, 1953.
(36) Müller, M.; Binder, K.; Oed, W. *J. Chem. Soc., Faraday Trans.* **1995**, *91*, 2369.
(37) Helfand, E.; Sapse, A. M. *J. Chem. Phys.* **1975**, *62*, 1329.
(38) Tanaka, K.; Taura, A.; Ge, S.-R.; Takahara, A.; Kajiyama, T. *Macromolecules* **1996**, *29*, 3040. Tanaka, K.; Takahara, A.; Kajiyama, T. *Macromolecules* **1997**, *30*, 6626.
(39) Palierne, J. F. *Rheol. Acta* **1990**, *29*, 204. Erratum: *Rheol. Acta* **1991**, *30*, 497.

MA020428D